



**HAL**  
open science

# Patient-specific finite element simulation of peripheral artery percutaneous transluminal angioplasty to evaluate the procedure outcome without stent implantation

Bernard Helou, Aline Bel-Brunon, Claire Dupont, Wenfeng Ye, Claudio Silvestro, Michel Rochette, Antoine Lucas, Adrien Kaladji, Pascal Haigron

## ► To cite this version:

Bernard Helou, Aline Bel-Brunon, Claire Dupont, Wenfeng Ye, Claudio Silvestro, et al.. Patient-specific finite element simulation of peripheral artery percutaneous transluminal angioplasty to evaluate the procedure outcome without stent implantation. *International Journal for Numerical Methods in Biomedical Engineering*, 2023, 39 (3), pp.e3685. 10.1002/cnm.3685 . hal-03970255

**HAL Id: hal-03970255**

**<https://hal.science/hal-03970255>**

Submitted on 12 Jun 2023




**HAL** is a multi-disciplinary open access archive for the deposit and dissemination of scientific research documents, whether they are published or not. The documents may come from teaching and research institutions in France or abroad, or from public or private research centers.

L'archive ouverte pluridisciplinaire **HAL**, est destinée au dépôt et à la diffusion de documents scientifiques de niveau recherche, publiés ou non, émanant des établissements d'enseignement et de recherche français ou étrangers, des laboratoires publics ou privés.



Distributed under a Creative Commons Attribution - NonCommercial - NoDerivatives 4.0 International License

# Patient-specific finite element simulation of peripheral artery percutaneous transluminal angioplasty to evaluate the procedure outcome without stent implantation

Bernard Helou<sup>1</sup>  | Aline Bel-Brunon<sup>2</sup>  | Claire Dupont<sup>1</sup>  | Wenfeng Ye<sup>3</sup> | Claudio Silvestro<sup>4</sup> | Michel Rochette<sup>3</sup> | Antoine Lucas<sup>1</sup> | Adrien Kaladji<sup>1</sup> | Pascal Haignon<sup>1</sup>

<sup>1</sup>Univ Rennes, CHU Rennes, Inserm, LTSI – UMR 1099, Rennes, France

<sup>2</sup>Univ Lyon, INSA-Lyon, CNRS UMR5259, LaMCoS, France

<sup>3</sup>ANSYS, Villeurbanne, France

<sup>4</sup>Medtronic, Aortic Peripheral & Venous (APV) Group, Santa Rosa, California, USA

## Correspondence

Bernard Helou, Univ Rennes, CHU Rennes, Inserm, LTSI – UMR 1099, F-35000 Rennes, France.

Email: [bernardhelou3@gmail.com](mailto:bernardhelou3@gmail.com)

## Funding information

ANR-11-LABX-0004; Région Bretagne

## Abstract

The purpose of this work is to present a patient-specific (*PS*) modeling approach for simulating percutaneous transluminal angioplasty (PTA) endovascular treatment and assessing the balloon sizing influence on short-term outcomes in peripheral arteries, i.e. without stent implantation. Two 3D *PS* stenosed femoral artery models, one with a dominant calcified atherosclerosis while the other with a lipidic plaque, were generated from pre-operative computed tomography angiography images. Elastoplastic constitutive laws were implemented within the plaque and artery models. Implicit finite element method (FEM) was used to simulate the balloon inflation and deflation for different sizings. Besides vessel strains, results were mainly evaluated in terms of the elastic recoil ratio (ERR) and lumen gain ratio (LGR) attained immediately after PTA. Higher LGR values were shown within the stenosed region of the lipidic patient. Simulated results also showed a direct and quantified correlation between balloon sizing and LGR and ERR for both patients after PTA, with a more significant influence on the lumen gain. The max principal strain values in the outer arterial wall increased at higher balloon sizes during inflation as well, with higher rates of increase when the plaque was calcified. Results show that our model could serve in finding a compromise for each stenosis type: maximizing the achieved lumen gain after PTA, but at the same time without damaging the arterial tissue. The proposed methodology can serve as a step toward a clinical decision support system to improve angioplasty balloon sizing selection prior to the surgery.

## KEYWORDS

atherosclerosis, percutaneous transluminal angioplasty, balloon sizing, acute post-procedural outcomes, patient-specific model, peripheral artery, finite element analysis

This is an open access article under the terms of the [Creative Commons Attribution-NonCommercial-NoDerivs](https://creativecommons.org/licenses/by-nc-nd/4.0/) License, which permits use and distribution in any medium, provided the original work is properly cited, the use is non-commercial and no modifications or adaptations are made.

© 2023 The Authors. *International Journal for Numerical Methods in Biomedical Engineering* published by John Wiley & Sons Ltd.

## 1 | INTRODUCTION

Atherosclerosis is the narrowing of vessel diameter due to atherosclerotic plaque. Peripheral arteries are one of the most vulnerable vascular locations for the occurrence of atherosclerosis. The development of this disease in femoral vessels for example is the main cause of claudication and critical limb ischemia (ischemic rest pain).<sup>1</sup> High numbers of hospitalized cases with relatively long stays are being reported every year as a result of atherosclerosis in lower-extremity arteries.<sup>2</sup>

Several treatment techniques are clinically available for atherosclerosis, each possessing its own advantages and limitations. Some are endovascular while others surgical. Being the minimally invasive option, endovascular techniques such as percutaneous transluminal angioplasty (PTA) are usually the favored alternative to invasive treatments for patients at higher risks of surgical morbidity and mortality.<sup>1</sup> Treatment via PTA consists of percutaneously inserting a balloon catheter within the stenosed arterial region, then inflating the balloon in order to damage/compress the plaque and widen the vessel lumen.<sup>3–5</sup> Stents may also be implanted subsequently. Their usage usually depends on the lumen patency attained immediately after PTA. Stent implantation had been showing better clinical outcomes in terms of elastic recoil in comparison to what is generally achieved with PTA alone.<sup>6</sup> However, being related to high rates of vessel injuries and in-stent restenosis (20%–40% of patients in femoral arteries for example at 2 years),<sup>1</sup> direct stents implantation after PTA is being re-questioned. Moreover, complex kinematics and small arterial dimensions (especially in peripheral arteries) increase the risk of stents fractures, calling for specific decisions for their usage.<sup>7</sup> Our primary interest being peripheral lower extremity arteries, this work is focused on the standard PTA technique, without stent implantation, because firstly, even if still not explicitly stated in publications (i.e., TASC II), it is the usual initial revascularization approach<sup>8,9</sup> and secondly, the development of drug-coated balloons makes it even more possible to retain sufficient dilation without stent.<sup>10,11</sup>

The success of PTA at short term is generally evaluated by the permanent lumen gained directly after the endovascular treatment. Apart from the compression and/or damage within the plaque, this phenomenon of non-recoverable deformation could also occur at the arterial level, clinically known by “controlled vessel injury”.<sup>12</sup> The resulting outcome is usually assessed by either the arterial patency, or the ERR measured at the maximum stenosed region after PTA, which characterizes how much the stenosed section recoils after balloon deflation. Therefore, anticipating clinical outcomes at short terms after PTA (residual deformations, elastic recoils, etc.) is essential for the treatment success evaluation, and could affect further treatment decisions (angioplasty, stenting, atherectomy, etc.). However, as detailed in Helou et al.,<sup>11</sup> among the various (generic/patient-specific) studies reporting the development of computational models for simulating PTA using finite element method (FEM), only few focused on modeling inelasticity (including plasticity) and evaluating outcomes at short terms after PTA alone.

Most studies were performed within idealized geometries. However, with simulations showing high sensitivity in results to small geometric and material properties changes,<sup>13</sup> FE studies are shifting recently more to patient-specific simulations. Among these patient-specific FE studies, some focused on evaluating plaque vulnerability and risk to rupture at normal blood pressures (without any supra-physiological loading caused by a balloon or a stent, etc.).<sup>14,15</sup> Others considered implanting stents before balloon deflation (balloon-expandable or self-expanding stents), hence not assessing residual deformations obtained immediately after PTA alone.<sup>7,16–18</sup> They focused mainly on stress distribution within stenosed arteries in relation to different stent designs, with results showing significant sensitivity. One main assumption restricting these FE studies from evaluating balloon angioplasty short-term outcomes is the elastic (linear or not) constitutive laws used for modeling arteries and plaques specifically. Without a stent implantation, elastic recoil after balloon deflation is theoretically equal to the gained deformation at max inflation (recoil of 100%), which contradicts clinical observations. According to clinical findings, elastic recoil immediately after PTA varies between 11% and 55% for different stenosed regions (size, shape and thickness), plaque compositions, and balloon/artery diameters ratios (i.e. Balloon Sizing).<sup>19–21</sup> Even though a recent generic study highlighted the importance of modeling residual deformations (and pre-dilations) toward endovascular treatment planning using FEMs,<sup>22</sup> up to our knowledge, very few patient-specific FE studies considered incorporating inelasticity with residual deformation within their models, and assessing outcomes directly after PTA alone.<sup>23–25</sup>

Moreover, among these studies,<sup>23–25</sup> none intended evaluating PTA outcomes (LGR, ERR, etc.) at short terms within femoral arteries specifically, despite being among the main revascularization approaches practically considered by clinicians at such arterial locations. Holzapfel et al.<sup>23</sup> was on an iliac artery; Gasser and Holzapfel<sup>24</sup> was a generic model mimicking a coronary artery; Decorato et al.<sup>25</sup> was in an arteriovenous fistula. Also, only one balloon sizing was

simulated within a particular stenosis case in each of the reported studies. Finally, except for the generic model of Liang et al.,<sup>26</sup> no FE study presents acute post-angioplasty simulated results in comparison with clinical outcomes.

In this work, our aim is to propose a patient-specific (*PS*) modeling methodology using implicit FE analysis, for simulating the PTA endovascular technique within a peripheral artery in order to evaluate the balloon sizing influence on its short term outcomes. Patient-specific 3D models were generated based on pre-operative computed tomography angiographies (CTA) corresponding to two femoral arteries. After assigning the calibrated material models for each artery and its respective plaque, a balloon was then inflated and deflated at different inflation diameters using FEM within both stenosed *PS* geometries. All chosen inflation diameters fall within the clinically recommended balloon sizing range (balloon/artery ratio) of [0.9 to 1.1] for PTA treatments.<sup>4</sup> For each patient at one specific balloon sizing, a comparison is presented between the simulated and its corresponding clinical outcomes obtained from 2D post-operative medical images. Then, besides analyzing generated vessel strains, results are evaluated in terms of ERR and LGR obtained along the stenosed arterial centerlines by comparing the pre and post-treatment geometries for each balloon sizing simulated within both patients.

## 2 | MATERIAL AND METHODS

### 2.1 | Geometry and Mesh

Preoperative Computed Tomography Angiography (CTA) images of two stenosed femoral arteries were obtained with ethical approval at CHU de Rennes and informed consent from participants: one with a dominant calcified atherosclerosis, while the other with a lipidic plaque. The CTA datasets (of 0.7 mm slice increment and thickness) were processed using the open-source softwares ITK snap and 3D slicer to generate models corresponding to each diseased artery. After selecting the desired regions of interest, the lumens were segmented using the snake active contour method implemented in ITK-snap.<sup>27</sup> With relatively high capabilities in absorbing x-rays, calcifications were also easily identified and segmented based on their high CT densities by thresholding. Then, subtract Boolean operations were applied in order to generate the lipidic plaque and the vessel walls, which are generally not clearly visible on CTA images. The procedure was the following: first the “healthy inner arterial walls” were created as the non-plaque equivalent by translating a constant diameter circle along the vessel centerline of each patient individually. Afterwards, the lipidic plaque of patient 1 was generated by subtracting its previously segmented PS lumen from its corresponding “healthy inner arterial wall.” Then with the considered vessel segments being rather short, constant vessel wall thicknesses of 0.9 mm versus 0.7 mm were initially modeled for patient 1 and patient 2, respectively. Finally, another subtract Boolean operation was performed to correct the vessel wall thickness of the calcified patient along its length, by removing the calcifications (when present) from its healthy arterial wall. Accordingly, segments corresponding to each plaque (lipidic in patient 1 while calcified in patient 2), in addition to the healthy arterial walls were obtained independently. Figure 1A, B present the two *PS* stenosed arterial reconstructed models showing the lipidic and calcified plaque cases respectively. Both segmented patient geometries were of varying stenosis severities reaching ~ 52% within the lipid plaque case and ~ 41% in the calcified one, at the most stenosed region. The calcified case had a more elongated distribution, so a 53.7 mm arterial segment was modeled to include the entire stenosed region. A shorter arterial segment of 34 mm in length was considered for the lipidic plaque case.

The artery and the plaque of both patients were meshed using hybrid solid elements in Ansys mechanical ensuring u-P mixed formulation. Following the mesh sensitivity analysis performed with the generic model presented in Helou et al.,<sup>11</sup> the *PS* stenosed artery with the calcified plaque was meshed by 773,230 4-node linear solid elements corresponding to typical element sizes of 0.24 mm for the entire geometry and 0.19 mm in the inner surface subjected to contact with the inflating balloon. A preliminary evaluation on a generic geometry showed indeed that linear elements performed equally well as quadratic elements but highly reduced the computational cost. Differently, having a smoother geometry with less sharp edges and irregular forms, the fine mesh sizes used within the calcified plaque case were not required within the lipidic one. Accordingly, in order to reduce the simulation time, another sensitivity study was performed on the mesh for the patient with the lipid plaque before executing the needed simulations for that case. The stenosed artery of this patient was consequently meshed by 272,991 4-node linear solid elements corresponding to 0.28 mm and 0.24 mm element sizes respectively for the whole model and in the stenosis inner surface in contact with the balloon. The new mesh-size convergence analysis (corresponding to the patient with the lipid plaque) is presented

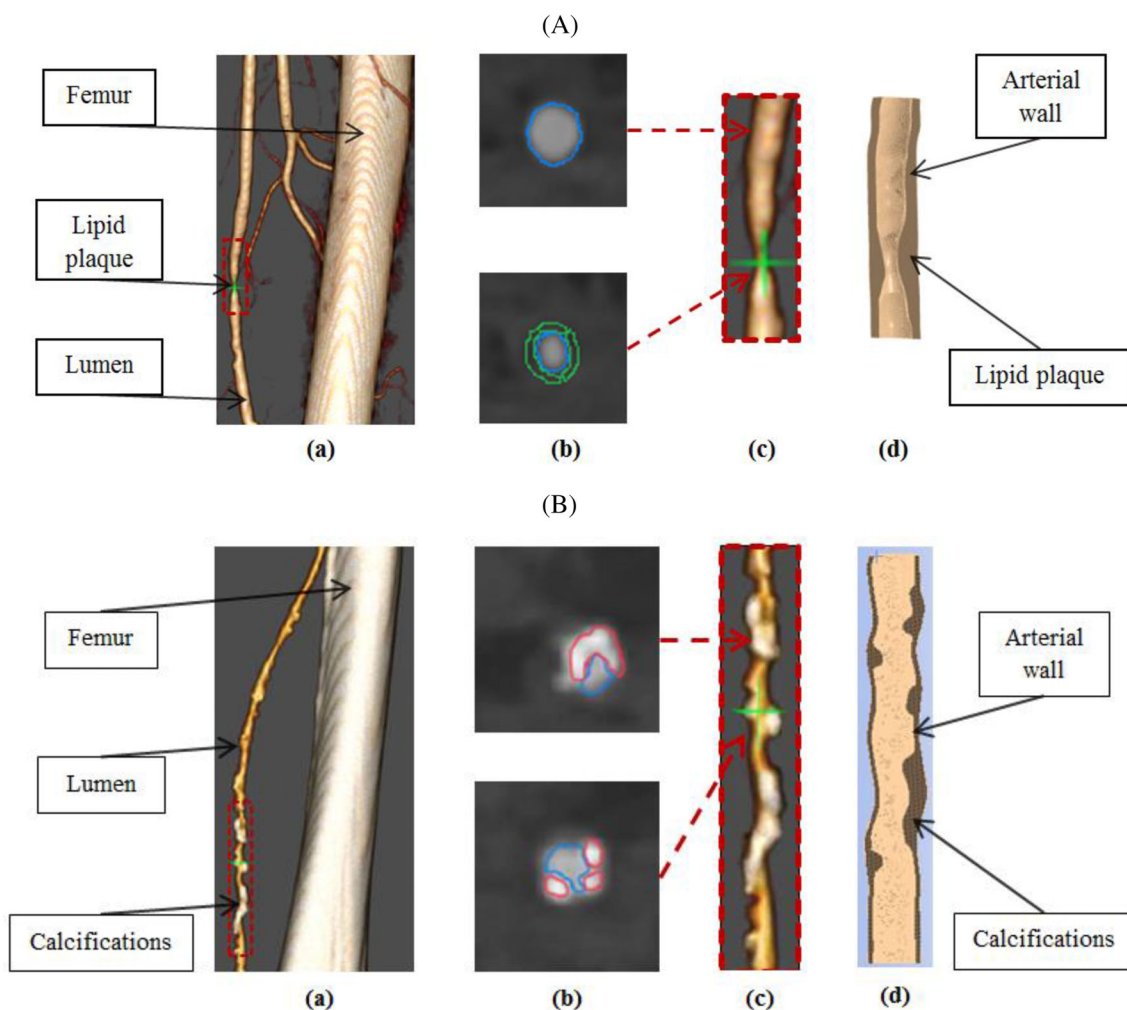


**FIGURE 1** Patient-specific femoral stenosis arterial models corresponding to the lipid (A) and the calcified (B) plaque cases respectively: (a) 3D observation of each stenosed artery and femur bone from CTA. (b) Pre-operative CTA axial slices at two different locations along each diseased artery, with the lumen, the lipid plaque, and the calcifications shown in blue, green, and red respectively. (c) 3D observation of each atherosclerotic region in a zoomed view, with the lumen seen in yellow, the calcifications in white, while the lipid plaques not represented. (d) A cross-sectional view at a random plane showing the plaque and the arterial wall of each reconstructed 3D geometry

in the appendix. In what follows, the patients with the lipidic and calcified stenosis would be referred to as patient 1 and patient 2, respectively. The 3D FEM models of the complete PTA system for both patients are shown in Figure 2.

## 2.2 | Constitutive Laws

With the purpose of the present work in modeling residual deformations and evaluating acute outcomes after balloon deflation, plasticity was included in the constitutive laws of the atherosclerotic components models. Material models implemented here were extracted from a previous work<sup>11</sup> based on generic simulations. As a recall, the plaque material parameters were first obtained from Maher et al.'s work<sup>28</sup> that experimentally reported the inelastic behavior of human atherosclerotic plaques under cyclic radial compressive loading regimes. Lipid and calcified plaques were considered for the calibration. Then, an intermediate simulation was set up to verify if these plaque parameters together with a hyper-elastic model for the artery would provide realistic results at unloading in comparison with clinically reported data. However, as the average luminal diameter loss, also referred to as the diametric ERR, resulting from the intermediate simulations exceeded the clinically expected ones, and as arterial tissues also experimentally show an inelastic

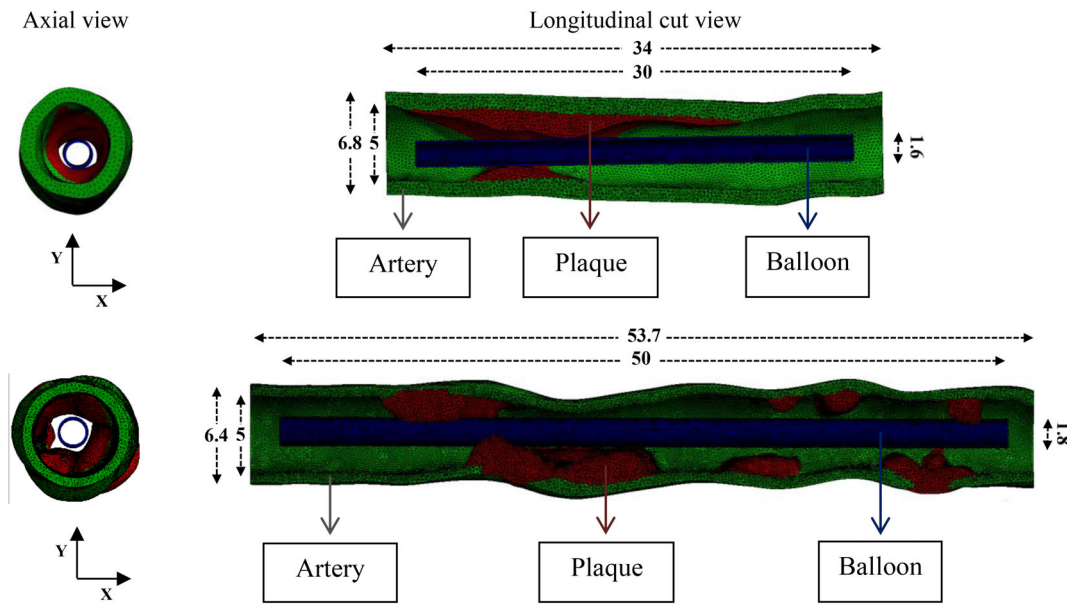


**FIGURE 2** Finite element model of the complete balloon angioplasty system within the two *PS* geometries at their initial state: the lipidic plaque case seen at the top, while the calcified one at the bottom. All dimensions are in mm

material behavior under supra-physiological loadings,<sup>29</sup> it was then hypothesized that the artery itself would also experience permanent deformations, and hence its plastic material parameters were tuned accordingly to satisfy averaged clinically reported ERRs for each plaque type respectively. It is important to notice that the parameters calibrated from generic simulations for both the plaque and the artery were kept identical in the present work; no further calibration was performed based on patient-specific simulations. Table 1 summarizes the material coefficients of the material models implemented in this work.

### 2.3 | Loading and Boundary conditions

The Medtronic Admiral Xtreme and the ULTRAVERSE 035 PTA balloon catheters were clinically deployed within patient 1 (with the lipidic plaque) and patient 2 (with the calcified atherosclerosis) respectively. The two 5 mm nominal diameter balloons were modeled as hollow cylinders of shell elements: the balloon implemented in patient 1 was modeled with an initial diameter of 1.6 mm and a length of 30 mm, whereas the one of patient 2 was modeled with an initial diameter of 1.8 mm and a length of 50 mm. The modeled initial diameter was defined as the crimped balloon diameter onto its catheter (i.e. approximately 1.6 mm for the Medtronic Admiral Xtreme vs. 1.8 mm for the ULTRAVERSE 035 one), while the simulated length was chosen enough to extend past the lesions on both sides, according to the manufacturers' recommendations.

With both balloons falling in between the semi and non-compliant balloon families following the relationship we proposed to categorize PTA balloons in Helou et al.,<sup>11</sup> and most importantly with no significant variation observed in

**TABLE 1** Material parameters of the lipid and calcified plaques and their corresponding arteries

Plaque type	Young modulus of elasticity E (MPa)	Poisson ratio ( $\nu$ )	Yield strength (KPa)	Tangent modulus (KPa)
Lipid plaque	0.105	0.40	5	62.77
Calcified plaque	0.189	0.40	15.79	111.88
Artery (lipid plaque case)	0.677	0.44	7	256.5
Artery (calcified plaque case)	0.677	0.44	7	330.75

the results of interest (ERR, LGR, etc.) when the balloon design changed as was reported for similar material models,<sup>11</sup> being the more robust method, both balloons were modeled here as displacement-driven non-compliant balloons. The balloons were initialized in a straight configuration and centered within the lumen. Driven by displacement, each node within the meshed balloon geometries was radially displaced until reaching the aimed balloon diameter for each simulated case before going back to its initial position. Accordingly, the two balloons would always reach the exact desired inflation diameters when simulated, independently of their thickness and initial diameters considered. Our balloon modeling choice was also in accordance with the studies of Holzappel et al.,<sup>23</sup> Grogan et al.,<sup>30</sup> and Conway et al.<sup>22</sup>

Being interested in balloon sizing influence analysis on acute PTA outcomes, six and ten balloons of different nominal diameters were simulated to their nominal values, and then deflated back to their initial position within patient 1 and patient 2, respectively. Tables 2 and 3 present the balloon sizing corresponding to each simulated diameter for patient 1 and patient 2, respectively. All simulated balloon diameters fall within the clinically recommended balloon sizing range (balloon/artery ratio) of [0.9 to 1.1] for PTA treatments.<sup>4</sup>

As proposed in Reference<sup>11</sup>, in-plane arterial translations (in  $x$ - $y$  plane) were allowed at both arterial ends to adapt to balloon radial inflation, with the balloon itself being clamped from both sides. Axial translation and rotation were blocked in the model as well. Moreover, no internal pressure was further considered at the stenosed arterial inner wall under the hypothesis that the CTA data (from which the  $PS$  geometries were generated) were obtained at normal blood pressure.

The non-linear contact between the balloon and stenosed artery is frictionless and formulated by pure penalty method. ANSYS implicit commercial finite element software (ANSYS<sup>®</sup> Academic Research Mechanical, Release 19.1.) was used to solve these large-deformation analyses.

## 2.4 | Analysis of results

To analyze balloon sizing influence on PTA outcomes, results were mainly evaluated in terms of the ERR and the LGR attained after balloon deflation. Elastic recoil is computed as the difference between the largest inscribed sphere

**TABLE 2** Balloon sizing at each inflation diameter simulated within the lipidic patient 1

Nominal diameter (mm)	Balloon sizing (balloon/artery ratio)
4.5	0.9
4.75	0.95
5.00	1
5.12	1.024
5.25	1.05
5.42	1.084

**TABLE 3** Balloon sizing at each inflation diameter simulated within the calcified patient 2

Nominal diameter (mm)	Balloon sizing (balloon/artery ratio)
4.5	0.9
4.625	0.925
4.75	0.95
4.875	0.975
5.00	1
5.06	1.012
5.12	1.024
5.23	1.046
5.33	1.066
5.42	1.084

diameter that can be generated along the centerline at max balloon inflation versus after balloon deflation (Equation (1)), while lumen gain is similarly assessed but after balloon deflation versus before balloon inflation (Equation (2)). *ERR* is comparable to what surgeons usually evaluate as a control for their clinical outcomes. *LGR* would be useful in interpreting the obtained elastic recoil in comparison to the stenosed arterial initial configuration. Lumen centerlines and max-inscribed-spheres were computed using the Vascular Model Toolkit library (VMTK—<http://www.vmtk.org>). Figure 3 presents an illustration of the inner luminal geometries of patient 1 showing the centerline and the max-inscribed-spheres appearing in two different positions along the stenosed artery, (a) before balloon inflation, (b) at its max inflation, and (c) after its deflation.

$$\text{Elastic Recoil Ratio in \%} = \text{ERR}_{\text{along\_centerline}} = \frac{D_{\text{max\_inflation}} - D_{\text{after\_deflation}}}{D_{\text{max\_inflation}}} \times 100, \quad (1)$$

$$\text{Lumen Gain Ratio in \%} = \text{LGR}_{\text{along\_centerline}} = \frac{D_{\text{after\_deflation}} - D_{\text{before\_inflation}}}{D_{\text{before\_inflation}}} \times 100. \quad (2)$$

### 3 | RESULTS

Several balloon sizings were simulated within each of the lipidic and calcified stenosed *PS* geometries. Results associated to patient 1 and patient 2 are presented in Sections 3.1 and 3.2, respectively.

#### 3.1 | Patient 1 with the lipid plaque

##### 3.1.1 | Simulation versus clinical outcomes

This patient was clinically treated using a balloon catheter inflated up to 5 mm and then deflated. Figure 4 A—I presents a 2D projection view of the injected lumen before PTA with a blue elliptical shape around its main treated region.

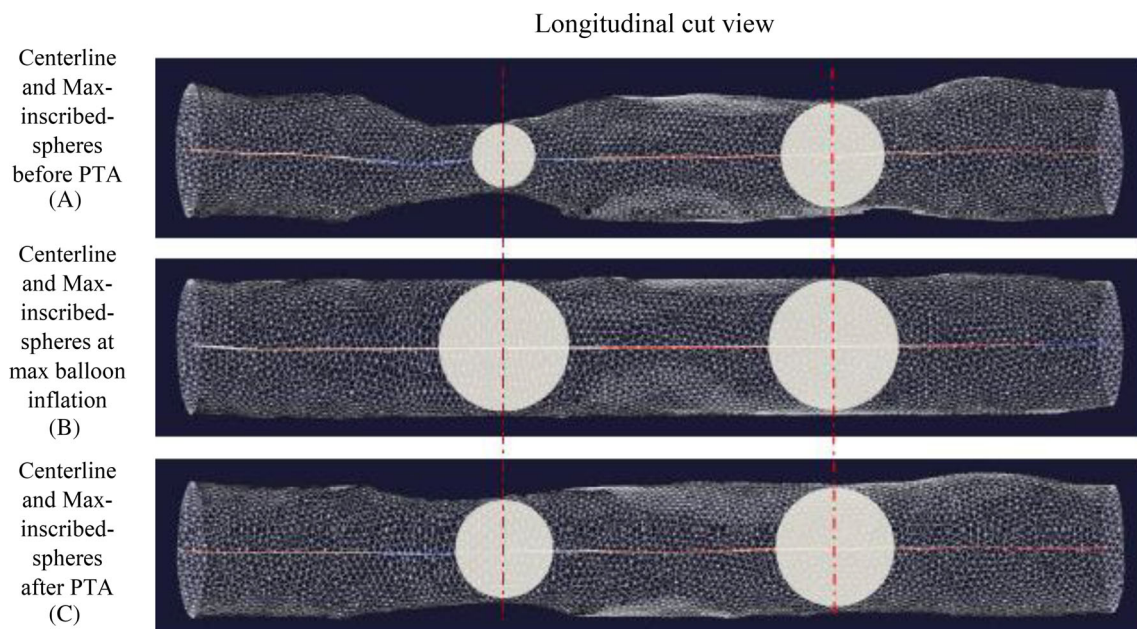


**FIGURE 3** Reconstructed surface geometries that correspond to the stenosed artery inner lumen of Patient 1 showing max-inscribed-spheres (in beige) at two random sections (in red) along their centerlines for the three states of interest during balloon angioplasty simulations

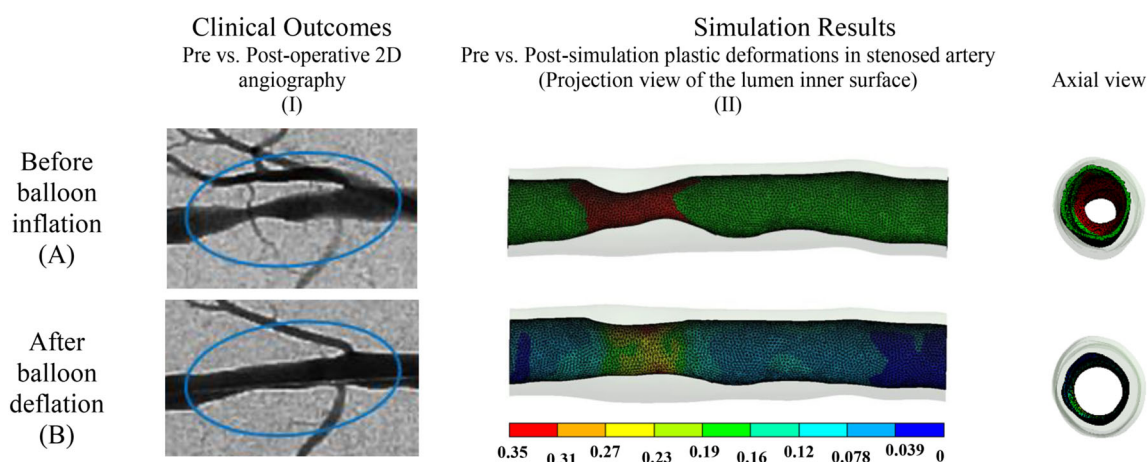


Figure 4 A—II shows another projection view of the lumen inner surface corresponding to the 3D stenosed femoral geometry generated from preoperative CTA of the same patient. The healthy arterial inner regions are seen in green, whereas the lipid plaque in red. Figure 4 B presents clinical and simulation outcomes obtained immediately after balloon deflation. Projection view of the injected lumen after PTA emphasizes the lumen gain along the treated region (Figure 4 B—I). The deflated balloon catheter can still slightly be seen in white. Figure 4 B—II displays the plastic strains computed in the simulated stenosed arterial model after balloon deflation. Quantitatively, a relatively small difference was observed in terms of residual stenosis after PTA upon comparing their values between the simulated and the clinical outcomes ( $\sim 25.5\%$  vs.  $28\%$ , respectively), both at the max stenosed region. Residual deformations can be clearly seen as well by comparing in axial view the arterial lumen before versus after balloon angioplasty simulation.

### 3.1.2 | Balloon sizing influence on post-procedural outcomes: LGR and ERR

Balloon sizing was evaluated by simulating angioplasty for six different balloon diameters within the range of clinically recommended balloon/artery diameters ratio. Figure 5 A presents the evolution of LGR along the artery axis and the corresponding initial lumen diameter. LGR directly evaluates the lumen dilation due to balloon inflation, that is, the presence of plastic strains within the tissues. As expected, LGR is noticeably larger where the initial lumen diameter is small (i.e., at main stenosis section) while it can reach 0 or even small negative values where there is no plaque. Negative values are probably due to surrounding plastic strains that can locally affect the artery diameter even in healthy sections. We can also see here that LGR is in positive correlation with balloon sizing, showing significant changes from one sizing to another. At the largest stenosed area for example, LGR locally reaches up to around 65% with the largest inflated balloon. Figure 5 B focuses more on the relationship between the LGR and the initial lumen diameter. For this patient, it can be seen that the dispersion of LGR is fairly small all along the treated region. This means that for such a patient, with a rather simple plaque geometry, the clinician can to a certain extent precisely control the attained LGR by driving the balloon expansion to the relevant sizing.

Unlike LGR that directly relates to the lumen expansion due to balloon inflation, ERR can be slightly more difficult to interpret when it comes to comparing sizings. ERR characterizes how much the stenosed artery recoils after being stretched by the inflated balloon; if the tissues were fully plastic, ERR would be 0. We can see in Figure 6 that ERR is maximum at the most stenosed region. Moreover, ERR increases with balloon sizing as well, which means that the



**FIGURE 4** Clinical versus simulation outcomes before (A) and after (B) balloon angioplasty. (A): Projection view of the injected femoral lumen before PTA (I) and another of its corresponding 3D geometric reconstruction (healthy arterial inner surface in green while the lipid plaque in red) (II). (B): Projection view of the same region after PTA illustrating its luminal gain (before catheter removal). Blue elliptical shape shows the main treated region (I). Simulation results also present the plastic strains resulting after balloon deflation with their effect on the final arterial lumen (II). Quantitatively, residual stenosis calculated after PTA from the clinical (I) and the simulated outcomes (II) were  $\sim 28\%$  versus  $25.5\%$ , respectively, both at the max stenosed region.

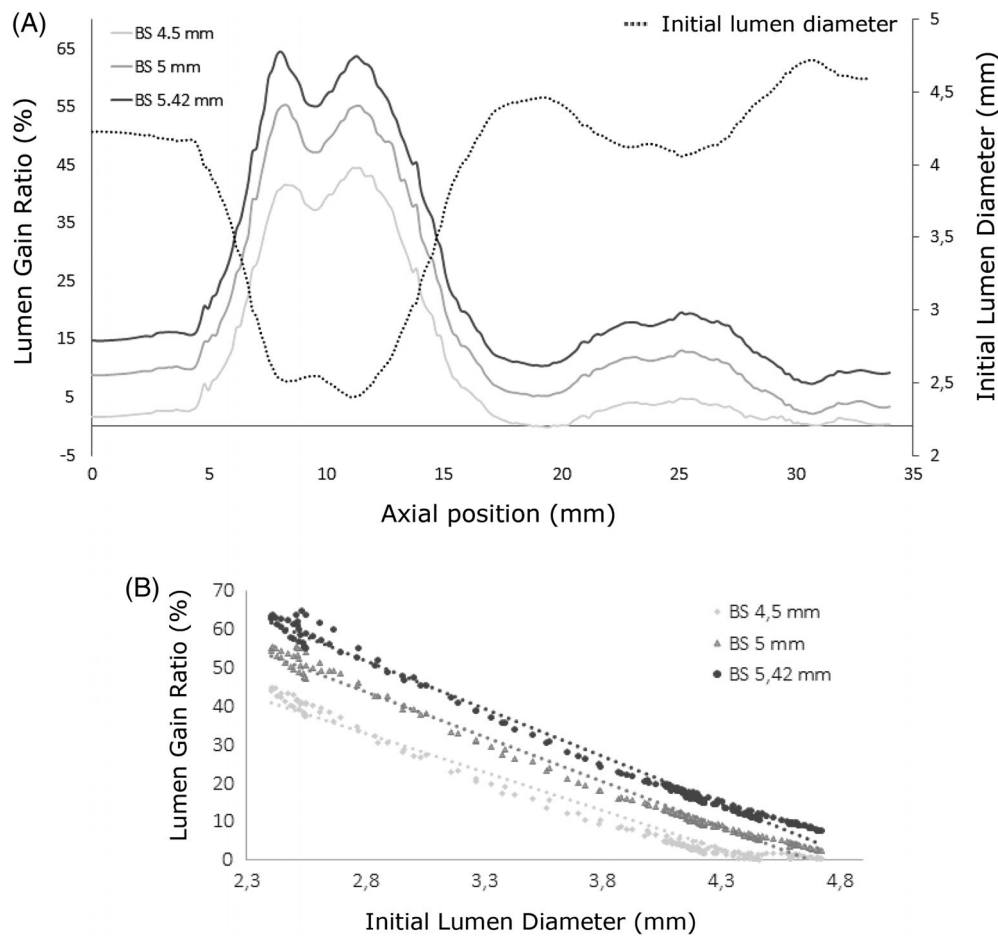


**FIGURE 5** (A): Lumen gain ratio for different Balloon Sizings (BS) and initial lumen diameter along the artery axis. (B): Attained lumen gain ratio (LGR) values for various initial lumen diameters along the arterial length, for different balloon sizings

stenosed artery experiences more elastic strain when balloon sizing increases. ERR does not indicate how much plastic strain the tissues have stored. Also, as the denominator  $D_{\max\_inflation}$  changes at each balloon sizing, it is not straightforward to explain the observed differences from one sizing to the other in terms of ERR, although it is typically the quantity that clinicians measure.

To evaluate which of the lipidic plaque and arterial wall is the most involved in the lumen gain, we have calculated the plastic deformation in both tissues over 5 mm-long portions of the model at 5 mm balloon sizing. Figure 7 presents the residual strain distribution within the two components in each 5 mm section along the arterial length. We can see that highest values of plastic strains forming within both components are attained at the most stenosed regions, i.e. in sections 5/10 and 10/15 mm. This confirms Figure 5 A which showed larger LGR values where the initial lumen diameter were small (i.e., within main stenosis segments as well). Moreover, as expected, the lipidic plaque stores larger amounts of plastic strain compared to the artery in similar sections; this is noticeably observed between 5 and 15 mm, always in the maximum stenosed region.

Finally, Figure 8 presents the evolution of the ERR and LGR together with balloon sizing, for three initial lumen diameters lying in moderately to largely stenosed areas within the patient with the lipid plaque. We can see in Figure 8 that both ERR and LGR are in direct correlation with balloon sizing, with significantly larger rates of change for the LGR in comparison to the ERR from one sizing to another. This indicates that increasing the balloon sizing to a large extent increases the LGR, and to a smaller extent increases the ERR. It also means that the stenosed vessel experiences more of both plastic and elastic strains with the increase of balloon sizing, with larger potentials of permanent deformations, that is, lumen expansion.

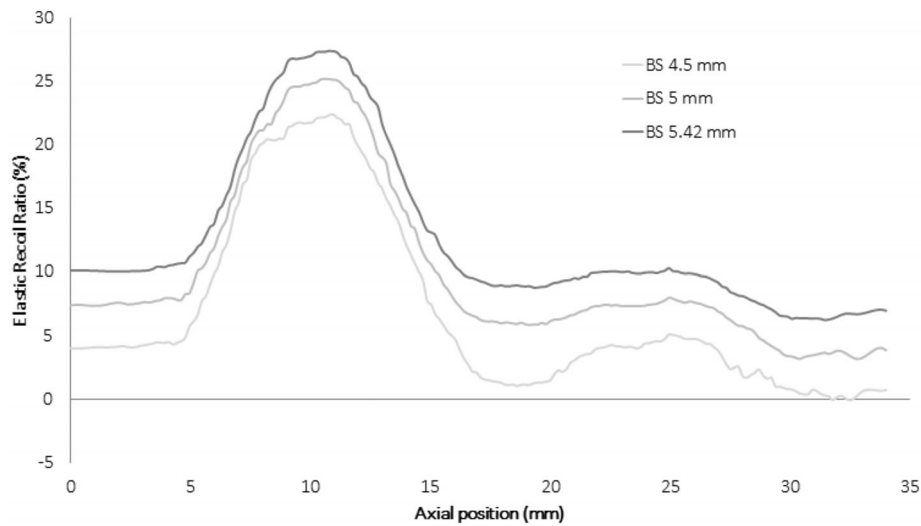


FIGURE 6 Elastic recoil ratio (ERR) evolution after PTA along the artery axis for diverse balloon sizings within the lipidic plaque case

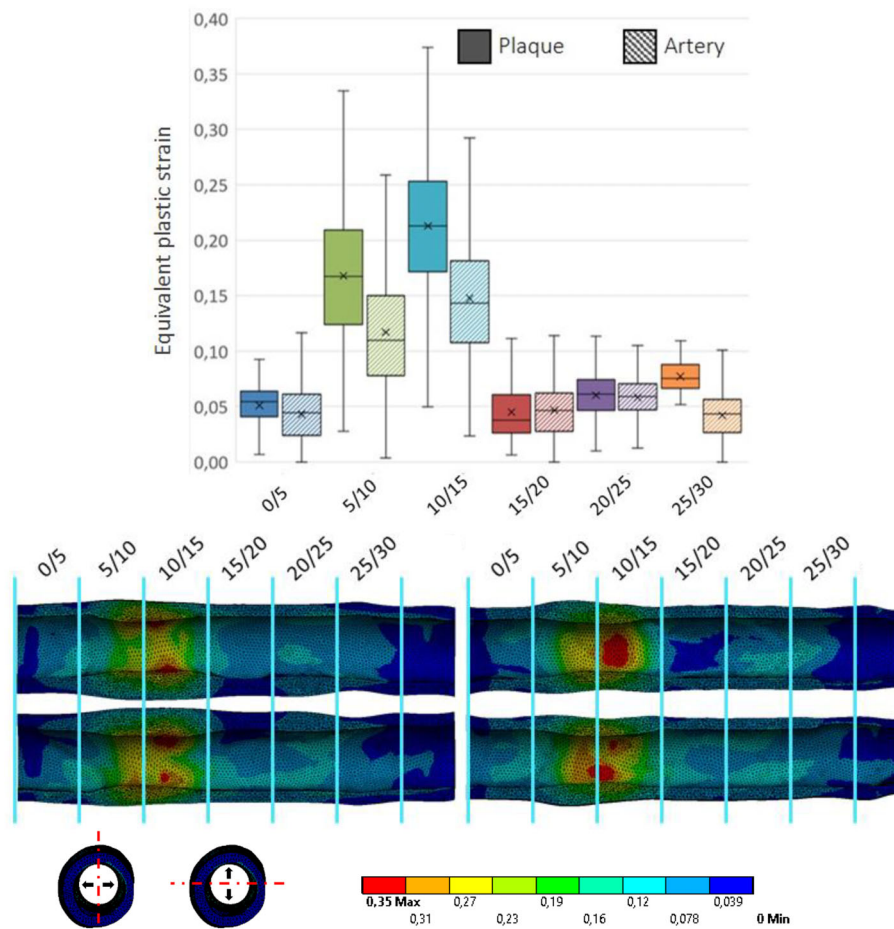


FIGURE 7 Distribution of the plastic strain stored in the lipid plaque and the arterial wall respectively. Each bar is calculated over a 5 mm-long section which axial position is indicated in mm below each couple of bars. The four cross-sectional views showing the plastic strain distribution within the stenosed artery correspond to the same PTA implantation phase (after balloon deflation) in four different orientations

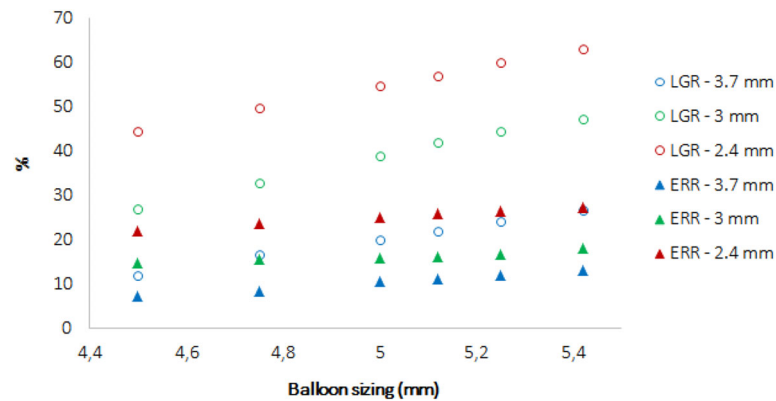


FIGURE 8 ERR and LGR evolution with balloon sizing for different initial diameters within patient 1

### 3.1.3 | Arterial wall max principal strain at max balloon inflation

Max principal strains forming in the external surface of the arterial walls at max inflations were compared for three different balloon sizing: 4.5, 5.12, and 5.42 mm. Results are depicted in Figure 9. In general the peak values occur at a similar location among the different sizings, within the max stenosed region.

## 3.2 | Patient 2 with the calcified plaque

### 3.2.1 | Simulation versus clinical outcomes

Clinically, this calcified patient was treated using a balloon catheter inflated up to 5.12 mm and then deflated. Similar to what was presented for the lipidic patient in Section 3.1.1, Figure 10 A—I illustrates a 2D projection view of the injected lumen before the treatment, with a blue elliptical shape around its stenosed region. Figure 10 A—II here shows a longitudinal cut view of the lumen inner surface corresponding to the 3D femoral geometry generated from preoperative CTA of this patient. Healthy arterial inner regions are seen in green, while calcifications in red. As for Patient 1, Figure 10 B presents clinical and simulation outcomes obtained immediately after balloon deflation. Projection view of the injected lumen after PTA illustrates the lumen gained along the treated region within this patient (Figure 10 B—I). The deflated balloon catheter was still present and is more visibly seen in white here. Figure 10 B—II displays the plastic deformations occurring in the simulated stenosed artery model after balloon deflation. Also here, at the max stenosed region of this patient, a relatively negligible difference was seen in terms of residual stenosis after PTA upon comparing their values between the simulated and the clinical outcomes ( $\sim 26\%$  vs.  $24\%$ , respectively). Permanent strains can also be clearly perceived by comparing in axial view the arterial lumen before versus after balloon simulation, for this patient as well.

### 3.2.2 | Balloon sizing influence on post-procedural outcomes: LGR and ERR

Balloon sizing was evaluated by simulating PTA for 10 different balloon diameters within this patient, also falling in the range of recommended balloon/artery diameters ratio. Figure 11 A shows the evolution of LGR and the initial lumen diameter along the artery axis corresponding to this calcified stenosis case. As expected, LGR was larger where the initial lumen diameter was small (large stenosis) while it reached 0 and even negative values where there was no plaque. Moreover, it can also be seen within this calcified patient that changing sizing in the recommended range significantly influences LGR as well. It more than doubled the LGR in largely stenosed areas, reaching locally around 30% with the largest balloon. Figure 11 B shows the relationship between the LGR and the initial lumen diameter within this patient. For highly stenosed areas (lumen diameter below 3.5 mm), the dispersion is small; it means that one can control more precisely the balloon sizing expansion to reach a targeted LGR. However this is less true here for larger initial lumen diameters; what happens in the mildly stenosed areas is usually clinically less crucial for the surgery

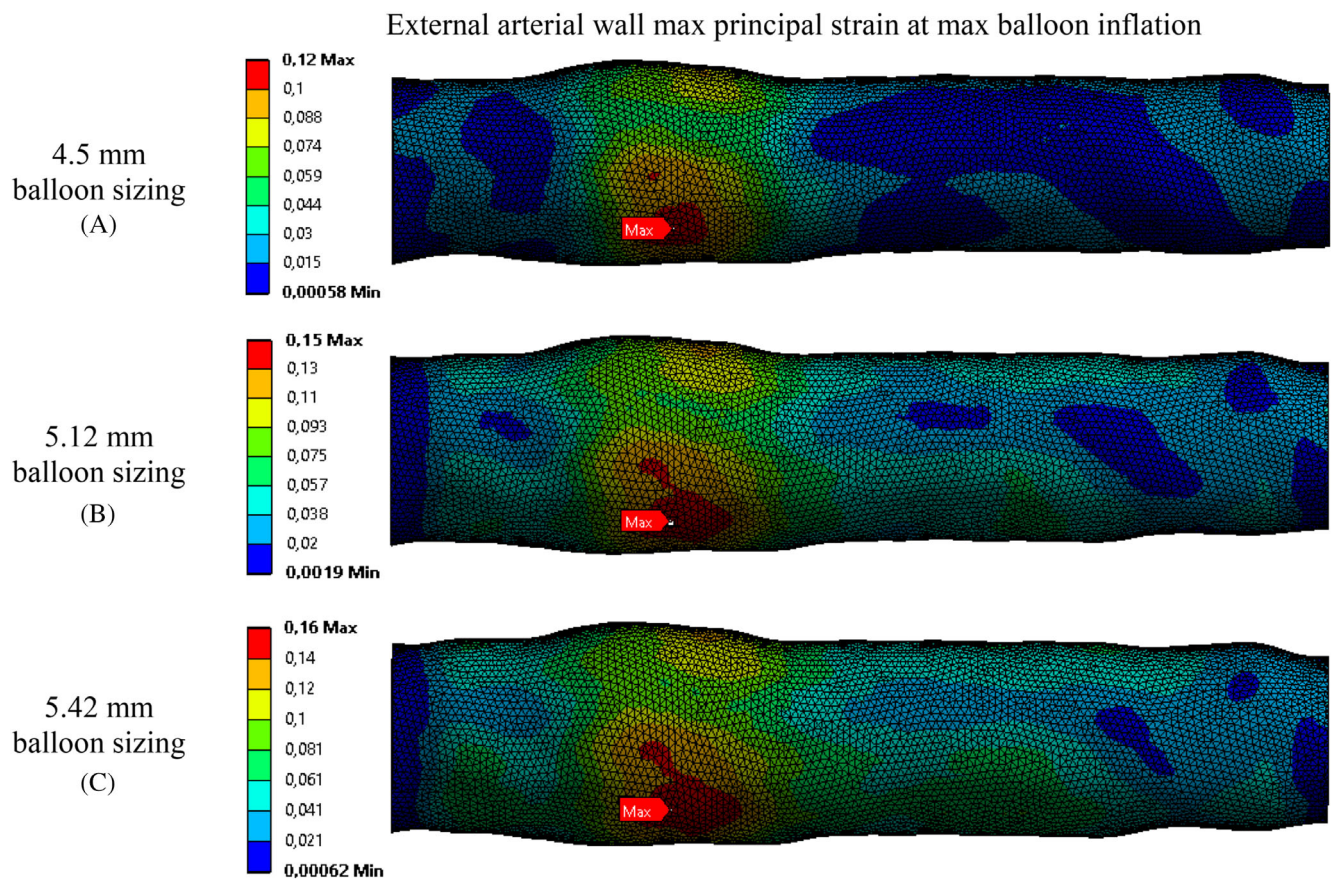


**FIGURE 9** Max principal strain field in the outer arterial wall during PTA at max balloon inflation for three different balloon sizing: 4.5 mm (a) 5.12 mm (b), and 5.42 mm (c). Max value site is also shown for each sizing

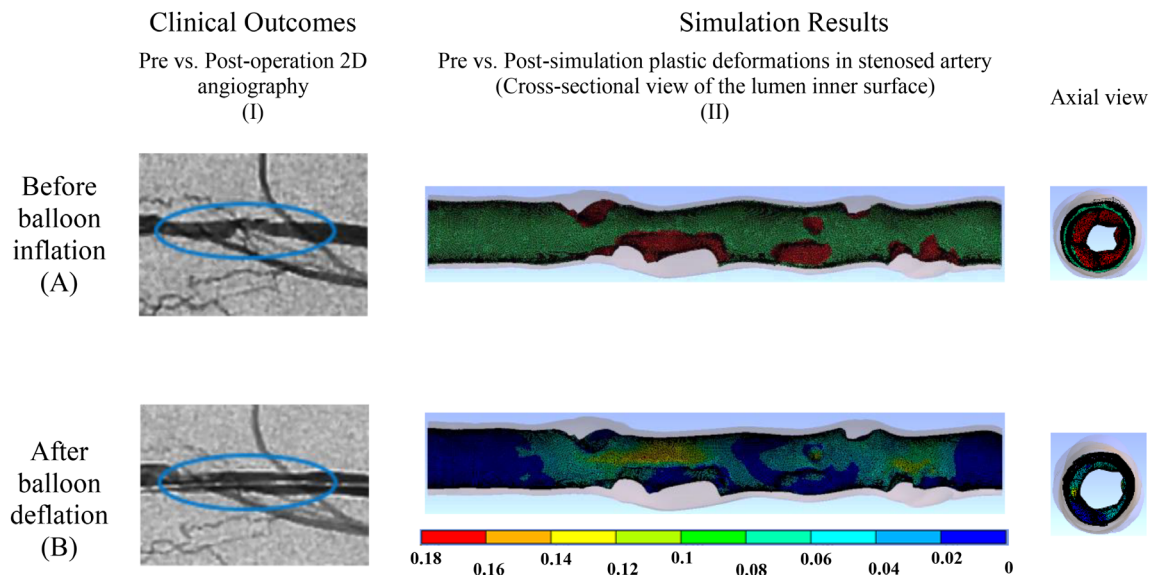


**FIGURE 10** Clinical versus simulation outcomes before (A) and after (B) percutaneous transluminal angioplasty. (A): Projection view of the injected femoral lumen before PTA (I) and a cross-sectional view of its corresponding 3D geometric reconstruction (calcified plaques in red while healthy arterial inner surface in green) (II). (B): Projection view of the same region after balloon angioplasty illustrating its luminal gain (before catheter removal). Blue elliptical shape shows the treated region (I). Simulation outcomes also present the residual deformations resulting after balloon deflation with their effect on the final arterial lumen (II). Quantitatively, residual stenosis calculated after PTA from the clinical (I) and the simulated outcomes (II) were ~ 24% versus 26%, respectively, both at the max stenosed region

success, but it is interesting to see that several locations of similar medium severity can experience, due to geometrical variations, dispersed outcomes in terms of LGR.

For the same reasons previously mentioned in Section 3.1.2, the interpretation of ERR can be slightly more challenging when it comes to comparing balloon sizings. Figure 12 presents the evolution of ERR along the artery axis for different balloon sizes and shows that it is in positive correlation with balloon sizing.

Also here, to evaluate which of the plaque and arterial wall is the most involved in the lumen gain, we have computed the plastic strain in both tissues over 5 mm-long portions of this model at 5 mm balloon sizing as well. We obtain the graph in Figure 13: it shows a large disparity in the plastic strain distribution in both the artery and the calcifications, which is more difficult to analyze for this patient. We can however draw some tendencies: in general, the artery experiences as much or more plastic strain than the calcified plaque. From 14 to 29 mm, two large plaque volumes are present; the transition from one to the other is in the 19/24 mm section, in which we observe a transfer of plasticity from the plaque to the artery. Also, in the 39/44 mm, there is just one medium-size plaque which stores a large amount of plastic strain, while the rest of the artery circumference is healthy. Hence besides observing that in general the arterial wall experiences more residual deformations in comparison to the calcified plaque within the various sections, it also seems that the more calcifications are present at different locations on the periphery of the section, the more plasticity is transferred to the arterial wall itself as well.

Finally, Figure 14 shows the evolution of the LGR and ERR together with balloon sizing for three different initial lumen diameters lying in moderately to largely stenosed areas. Even though the LGR values obtained here are relatively

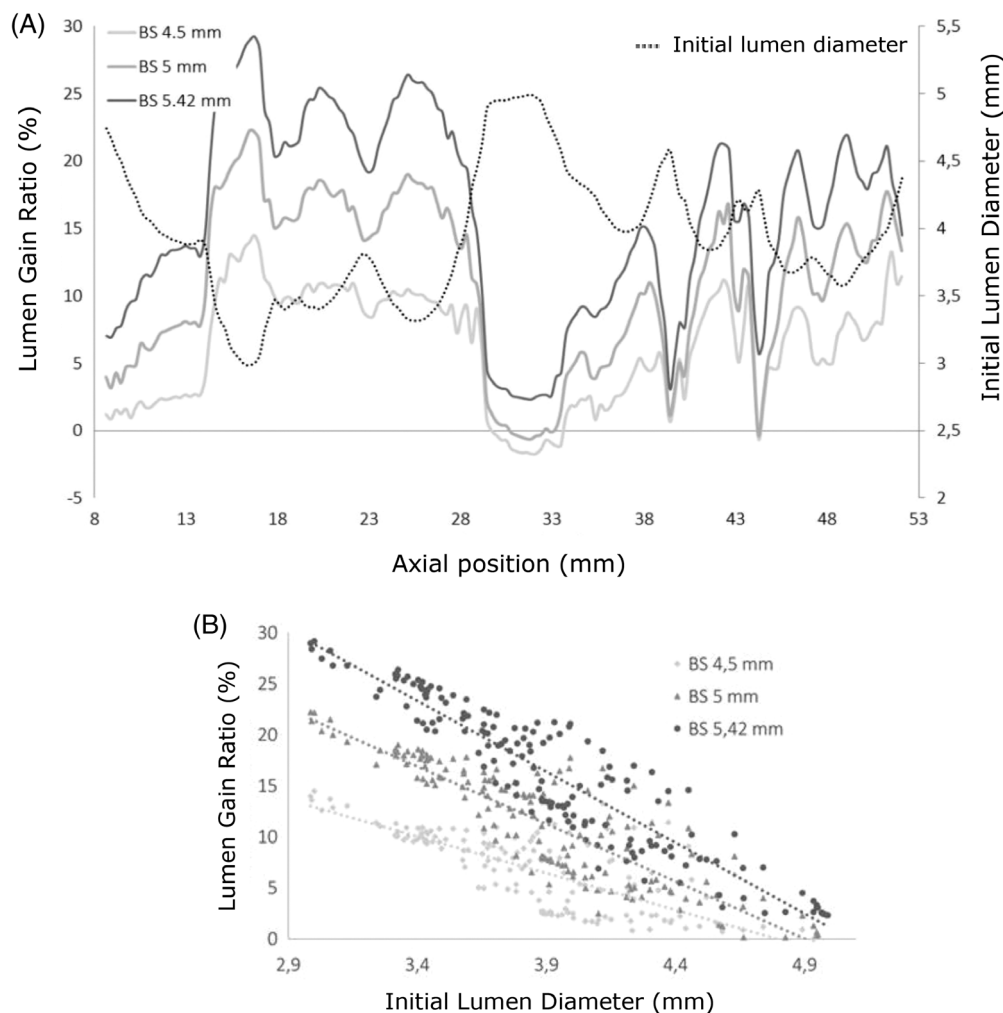


**FIGURE 11** (A) LGR for different balloon sizings in addition to the initial lumen diameter along the artery axis. (B): Obtained LGR for various initial lumen diameters along the artery, for different sizings of the balloon

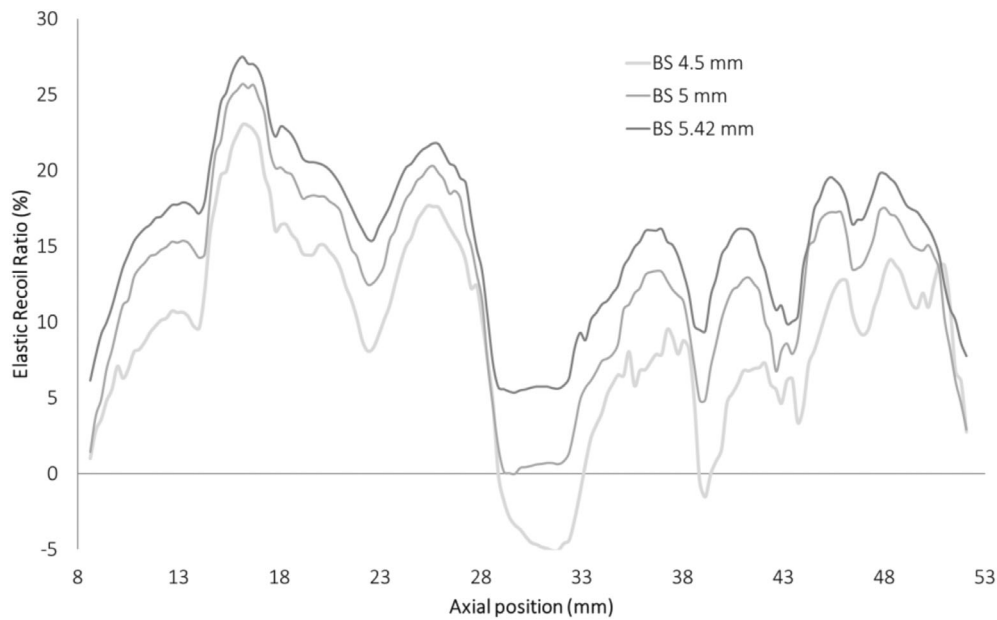


FIGURE 12 ERR evolution after balloon angioplasty along the artery axis for different balloon sizings within the calcified plaque case

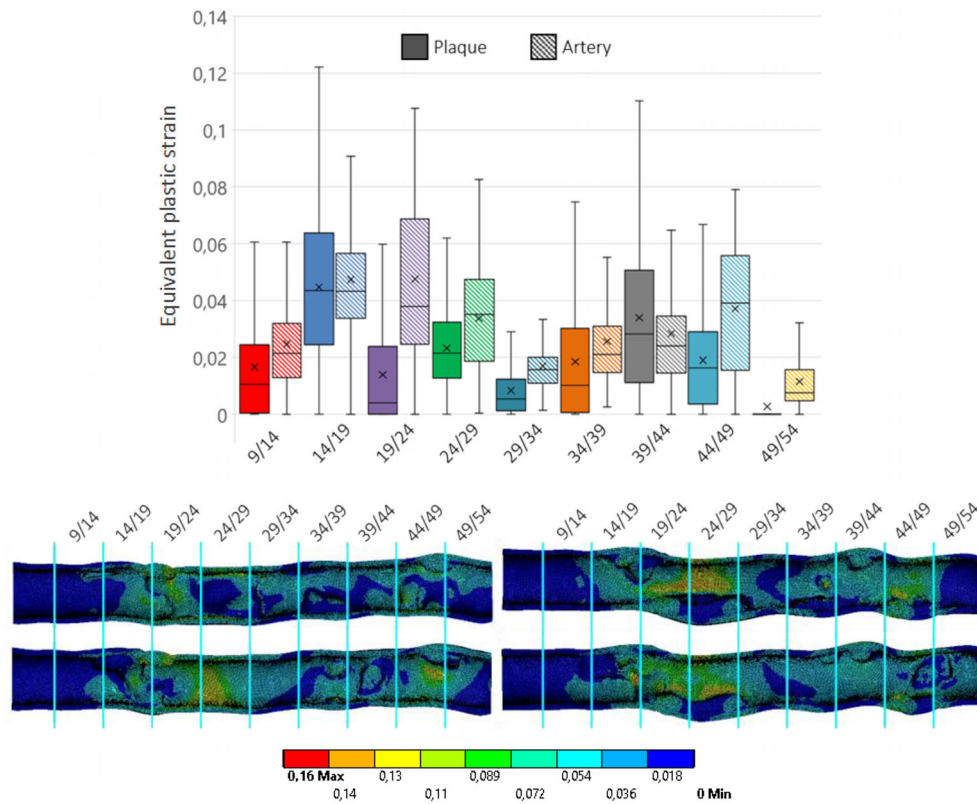


FIGURE 13 Distribution of the plastic strain stored in the calcified plaque and the arterial wall respectively. Each bar is calculated over a 5 mm-long segment which axial position is indicated in mm below each couple of bars. The four cross sectional views showing the plastic strain distribution within the stenosed artery correspond to the same PTA implantation phase (after balloon deflation) in four different view angles

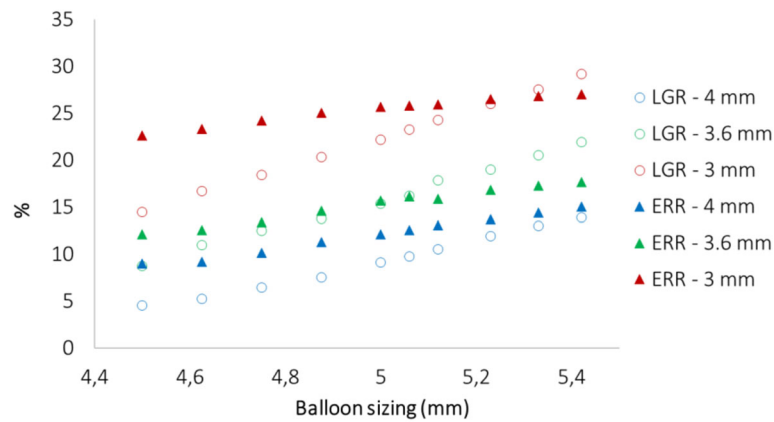


FIGURE 14 LGR and ERR evolution with balloon sizing for different initial diameters within patient 2

smaller than those of the lipidic case (seen in Figure 8), the graph below confirms that increasing the balloon sizing would to a large extent increase the LGR and to a smaller extent increase the ERR.

### 3.2.3 | Arterial wall max principal strain at max balloon inflation

Figure 15 illustrates the max principal strains distributed within the outer arterial wall at max inflation, for the three balloon sizings: 4.5, 5.12, and 5.42 mm. In comparison to the lipid stenosis case presented in Section 3.1.3, max principal strains peak values here show a more significant increase at larger diameters simulated: (0.27 at 5.42 mm vs. 0.16 at 4.5 mm).

The peak value location (labeled in red) seems to change within this patient for different balloon diameters; however, the three presented cases indicate that the peak value always occurs around the same axial cross-sectional area along the arterial length, that is, also at max stenosed region.

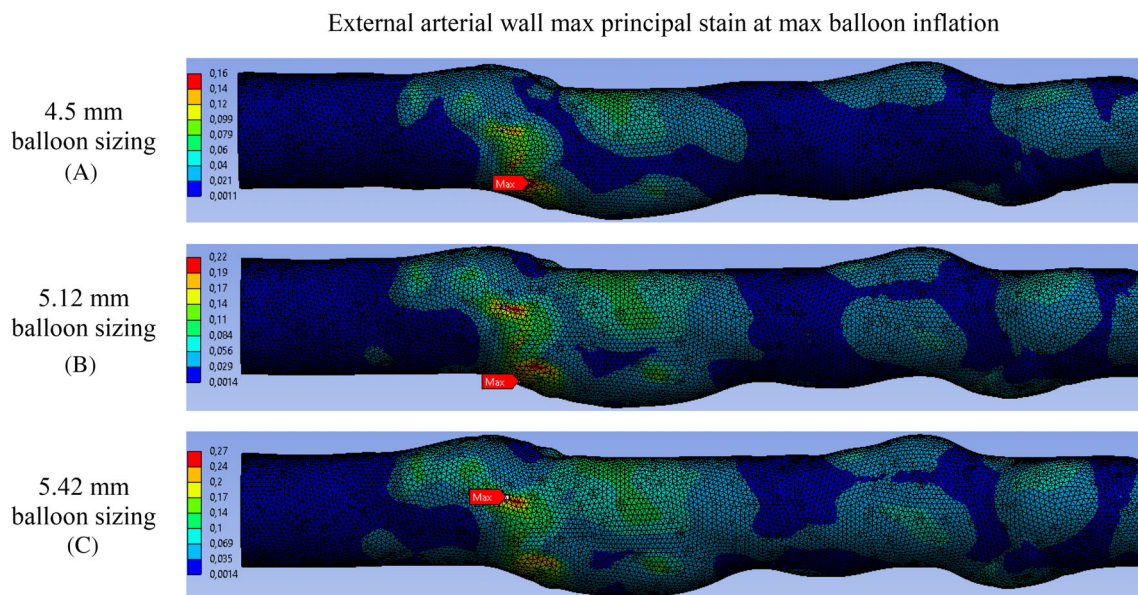


FIGURE 15 Max principal strain field in the outer arterial wall at max balloon inflation during angioplasty for the three different balloon sizing: 4.5 mm (a) 5.12 mm (b) and 5.42 mm (c). Max value location is marked for each sizing



## 4 | DISCUSSION

The present article aims at presenting a patient-specific modeling approach using implicit FEM for evaluating acute outcomes of a PTA procedure for different balloon sizings. Elasto-plastic constitutive laws were used for both the artery and plaque to model residual deformations. Results were mainly assessed in terms of ERR and LGR on two peripheral stenosis cases, one with a lipidic plaque while the other with calcifications; the distributions of plastic strains and maximal principal strains within the stenosed arteries and outer arterial walls were evaluated as well.

The balloon was initially driven up to 5 mm within the lipidic femoral geometry (patient 1), while to 5.12 mm within the calcified one (patient 2), and then deflated back to its original position in both cases. These inflation diameters were chosen in accordance with what was clinically performed for each patient separately. For both patients, a comparison between clinical and simulation outcomes before versus after PTA shows residual deformation development in the stenosed regions after balloon deflation (Figures 4 and 10). Permanent deformations can be clearly observed in the axial views of our simulations results. This observation is in accordance with FE studies that reported the presence of lumen gain within the vessel after PTA alone, even if these studies were not performed using in-vivo input imaging data.<sup>23,24,31</sup> Moreover, negligible differences in residual stenosis were obtained when comparing clinical versus simulation outcomes for each patient after PTA at its max stenosed region, showing that our constitutive models seem reasonable.

With the wide dispersion of calcifications within patient 2, both ERR and LGR curves showed several oscillations along the diseased artery accordingly with the plaque severity initial distribution. A similar behavior was observed on the corresponding curves of patient 1, but with noticeably fewer fluctuations throughout the arterial length being composed of a more concentrated plaque. However for both patients, ERR and LGR displayed a negative association to the initial lumen diameter variation along the stenosed region. This indicates that as expected, the most stenosed regions (smallest initial lumen diameters) are usually the most vulnerable to endovascular treatments; it corroborates the fact that treatment outcomes are usually clinically evaluated at such regions as well.<sup>3,19,20</sup>

Both ERR and LGR attained shortly after balloon angioplasty showed direct correlations to the increase in balloon inflation diameters within the two patients. This finding is in accordance with clinical results reporting positive association between balloon sizing and degree of elastic recoil.<sup>19,20,32</sup>

When analyzing clinically reported ERRs<sup>19–21,33</sup> in association to values obtained from our *PS* simulations, it also confirms that the calibration for the constitutive laws of the plaque and artery described in Helou et al.<sup>11</sup> and considered in this work is rational. Isner et al.<sup>33</sup> reported an average ERR of  $28.6\% \pm 7.2\%$  after PTA in iliac arteries. At similar locations, Gardiner et al.<sup>19</sup> measured  $36\% \pm 11\%$  as loss in luminal diameter after balloon deflation (ERR). Our ERR values computed at most stenosed sections after angioplasty, as usually measured by clinicians, ranged between 22% and 27.5% within both patients for the different balloon sizings simulated, thus showing consistency with clinical findings.

As a supplementary assessment for our simulation results, we also reported the LGR values attained by the two patients at similar sites (max stenosed regions). For the balloon diameters driven in this work, LGR ranged between 42% and 63% within the lipidic patient; while between 14.5% and 29.2% within the calcified one. It is noticeably higher between the two simulated patients here when the plaque is lipidic in comparison to when it is calcified. This finding is qualitatively in accordance with the clinical experience observed in our hospital center. In addition, quantitative clinical findings stated in the literature showed a large variety in their reported LGR values as well: for example 28.5% with,<sup>5</sup> while 110% with.<sup>34</sup> It is important to mention that from the way LGR is computed (seen in Equation (2)), besides atherosclerotic tissue composition and balloon sizing effects, we expect it to be also directly dependent on the initial geometric features of the stenosis (i.e., shape, distribution, and mainly severity). Recall that the two patients here had plaques of different distributions, shapes and severities, with patient 1 having the more severe plaque. Their arterial dimensions were initially not the same as well. Accordingly a direct one-to-one LGR comparison between the two cases here would not be relevant.

To better understand the behavior of the stenosed artery subjected to PTA, a statistic evaluation of plastic strain distribution within both the artery and the plaque is proposed for each patient individually at 5 mm balloon sizing. This evaluation helps understanding the phenomena at stake within the plaque and the artery: for a given lumen gain, it is interesting to see which of the artery and the plaque experienced the largest amount of permanent strain, depending on the plaque constitution and distribution in the observed location. If the plaque is the most permanently deformed, it could illustrate a higher risk of debris formation; if the artery is the most deformed, then it could correspond to a higher

rupture risk. Plastic strains were mostly stored within the main stenosed regions of both patients. At these locations, it can be observed that significantly higher residual deformations were formed in the plaque of the lipidic patient compared to its corresponding arterial wall; however, with more equally distributed plastic deformations within the components of the calcified case, it seems that large calcifications are rather more resistant to balloon pressure and promote more transfer of plastic strains to the artery. It can be seen that predicting which of the plaque or the artery would experience the more plastic deformation is not always straightforward; more patient data would be necessary to quantitatively confirm the hypothesis of the calcified case. Last, the noticeably larger magnitude ranges of plastic strains stored within the stenosed region of patient 1 confirms the significantly larger LGR values reported for the same patient as discussed in the previous paragraph.

Patient 1 showed higher LGR magnitudes compared to ERR at similar axial locations within the treated artery. Differently, patient 2 in general showed higher ERR values with respect to LGR instead. Nevertheless for both patients, with the balloon sizing growth, the increase in ERR became limited compared to the rise in LGR, particularly at highly stenosed regions; they do not evolve at the same rate with respect to sizing, which makes sense given their expression. Indeed, on the max stenosed section, for an augmentation of balloon diameter from 4.5 to 5.42 mm, the ERR was increased from 22% to 27% with the lipidic patient and from 23% to 27.5% with the calcified one, while the LGR rose from 42% to 63% with the lipidic case and from 14.5% to 29.2% with the calcified one. Firstly it seems rational that, given arterial elastic properties, any increase in arterial stretching would lead to a growth in elastic recoils.<sup>19</sup> However the small rise in elastic recoil compared to lumen gain indicates that the treated stenosed arteries evolve mostly in their plastic range of deformation at higher balloon sizing, showing more permanent deformations than elastic ones.

Damage assessment is a critical issue in the prediction of clinical outcomes. It can be considered as a positive observation by clinicians (“controlled vessel injury” enhancing resulting lumen after PTA) until it starts risking the artery itself from being injured. In this work, we do not claim to model the detailed damage phenomenon that might occur during balloon angioplasty. Plasticity was considered instead to approximate complex damage and flow phenomena occurring in stenosed arteries at small scales. Showing coherent results in comparison with clinical outcomes, our implemented model seems to be promising for ERR and LGR assessments after PTA. In this work, any increase in plastic deformations (quantified by LGR augmentation), is an indication of the presence of more damage within treated region at higher balloon sizing.

Max principal strains at max inflations showed wider distributions along the outer arterial walls of both patients for higher balloon sizings. Here, max principal strains in the external surface of the arterial walls were considered for the assessment of their risk of rupture. It can be observed for the two patients as well, that the magnitude of their peak values also increased at higher inflation diameters, but with a sharper increase with the calcified plaque. Strain peak values increased from 0.16 to 0.22 to 0.27 when the plaque was calcified versus from 0.12 to 0.15 to 0.16 when the plaque was lipidic, respectively, for the three different evaluated sizings. It seems that augmenting balloon sizing during PTA would place the arterial wall at higher risks to rupture when the treated plaque is calcified than when it is lipidic soft. Increasing balloon sizing seems to be a safer option for clinicians toward enlarging the lumen gained within a lipidic stenosis compared to a calcified one.

Moreover, within the lipid plaque, strain peak values occurred at a similar location of maximum stenosis for the three sizings. For the calcified case, even though their locations seemed to vary among the different sizings, they all ended up occurring around the same axial position, where the stenosis severity was maximal initially. Therefore, despite showing the highest LGRs with balloon sizing increase for both plaque types, arterial walls at maximum stenosed regions were most likely to experience the highest max principal strain values during inflation as well. This indicates that a compromise should be considered for each stenosis type, maximizing the achieved lumen gain after PTA from one side, but at the same time without damaging the healthy arterial tissue. Hence, selecting the max possible balloon sizing that would not put the treated region under the risk of rupture should be the adequate sizing choice toward clinical outcomes optimization. Threshold values setting arterial risks of rupture should be further defined for an appropriate balloon sizing selection.

Limitations of the present work principally concern the plaque and artery models, as previously detailed in Helou et al.<sup>11</sup> In summary, in this work we do not claim to model the detailed phenomena of damage that might occur during PTA. Instead, plasticity is meant to model any complex damage and flow phenomena occurring at small scales within the diseased artery. Besides, using a bilinear elasto-plastic constitutive law for the artery (and the plaque) was a way to limit the number of coefficients to calibrate. We assumed that the first part of this law represented the tangent behavior of the artery between its prestressed state due to blood pressure and the supra-physiological state due to balloon

inflation (before plasticity) and that the difference between this tangent (stiff) linear behavior and a more realistic nonlinear stiffening behavior could be considered as a second-order factor. Also, the calibration of the proposed constitutive laws is mostly based on kinematic quantities, such as residual strains extracted from Maher's work and the clinical ERR provided by different papers, toward the main scope of this article: to evaluate acute outcomes (primarily ERR and LGR) after PTA. The proposed model might require further validation to assess other interesting quantities during large (supra-physiological) loading such as the arterial risk of rupture based on maximum stress.

Modeling the plaque as a single component is a simplification here as well. The reason for this choice was first, that according to the clinical experience in our hospital center, femoral artery plaque is generally homogeneous when it requires treatment, and it is usually evaluated as being either calcified (stiff) or lipidic (soft), rather than with multi-components as seen in other stenosed regions.<sup>35,36</sup> The second reason is that we aim to develop a tool that can be integrated into the clinical routine without any additional imaging. We can clearly see in Figures 1, 4 and 10 that the spatial resolution and contrast of routine images currently do not allow for a detailed multi-component plaque geometry. Similarly, at their current state, they do not allow either for a differentiation among the three common arterial layers. Accordingly, a single-layered artery was considered in this work.

We are also aware that modeling the artery as a single-layer tissue is a limitation, being known to be composed of the three common layers: the intima, the media and the adventitia. However, even though in-vitro experimental studies evaluating atherosclerotic tissues behaviors are generally available in the literature, only a few among them considered studying the inelastic behavior of such tissues. Up to our knowledge, no study presented the inelastic behavior of each arterial layer separately under supra-physiological loadings. Accordingly, with the lack of the necessary experimental data that represent the layer specific inelastic behaviors of arteries, in this work, an inelastic single-layered artery was considered and was tuned correspondingly to model permanent deformations obtained directly after PTA.

Another simplification here is neglecting blood pressure effect on the *PS* geometry by considering the imaged geometry (the one that we segmented) to be similar to the geometry without blood pressure. We consider here this assumption acceptable as our constitutive law is linear in its elastic phase (refer to<sup>11</sup> for more details), so the stiffness is rather larger starting from the 0-stress configuration. However, further validation of the effect of the physiological blood pressure on acute outcomes after PTA might still be required at this stage for more precision, as we expect plastic strains to possibly occur sooner if the simulation is run from a configuration pre-stressed by blood pressure.

Despite the mentioned simplifications, with consistency being shown between simulations results and clinical outcomes, our model seems to be promising toward ERR and LGR assessments after balloon angioplasty.

## 5 | CONCLUSION

This work presents a new approach for the evaluation of angioplasty balloon sizing influence on outcomes immediately after the treatment of a patient-specific femoral artery. It is based on the combination of implicit structural finite element analysis, material calibration (not presented here) and medical image analysis. Higher plastic strains (and LGR accordingly) were shown within the stenosed region of the lipidic patient. Simulated results also showed a direct and quantified correlation between balloon sizing and each of the attained ERR and LGR after PTA for both patients, with a more significant influence on the lumen gain. The max principal strain values in the outer arterial wall augmented at higher balloon sizes during inflation as well. Their rates of increase were higher when the plaque was calcified. The maximal LGRs were attained at the same axial position where the peak strain values were observed; they both coincided with the initial max stenosis severity location. Therefore, our model shows that despite enhancing the resulting lumen after PTA, excessive balloon sizing might place the treated artery at more injury risks, with higher ones when the plaque is calcified. Results also illustrate that increasing balloon sizing can be the better choice toward optimizing acute outcomes after PTA (more safely maximizing lumen gain) within a lipidic plaque compared to a calcified one. The next step is to evaluate the proposed method as a component of a decision support system providing the clinician with a mean to enhance clinical outcomes by objectively selecting the max balloon sizing that would not risk rupturing the treated region. To this aim, further validation of our model parameters will be conducted using pre- and postoperative clinical data on several cases of different arterial dimensions, plaque severities, plaque compositions. Arterial rupture threshold values should also be further defined for a more precise balloon sizing selection.

## ACKNOWLEDGEMENT

This work was partially supported by the Bretagne region and by the National Research Agency (ANR) in the framework of “Investissement d’Avenir Program” through Labex (ANR-11-LABX-0004). We thank Nicolas Courtial from LTSI lab for his support on VTK files format.

## DATA AVAILABILITY STATEMENT

The data that support the findings of this study are available on request from the corresponding author. The data are not publicly available due to privacy or ethical restrictions.

## ORCID

Bernard Helou  <https://orcid.org/0000-0002-7633-3798>

Aline Bel-Brunon  <https://orcid.org/0000-0002-2398-9064>

Claire Dupont  <https://orcid.org/0000-0002-7727-3846>

## REFERENCES

- Cunnane EM, Barrett HE, Kavanagh EG, Mongrain R, Walsh MT. The influence of composition and location on the toughness of human atherosclerotic femoral plaque tissue. *Acta Biomater.* 2016;31:264-275. doi:10.1016/j.actbio.2015.11.056
- Jaff MR, MacNeill BD, Rosenfield K. Angiography of the aorta and peripheral arteries. In: Baim DS, ed. *Grossman's Cardiac Catheterization, Angiography, and Intervention.* 7th ed. Lippincott, Williams & Wilkins; 2006:254-280.
- Baim DS. Percutaneous balloon angioplasty and general coronary intervention. In: Baim D, ed. *Grossman's Cardiac Catheterization, Angiography, and Intervention.* 7th ed. Lippincott, Williams & Wilkins; 2006:433-466.
- Safian RD, Hoffmann MA, Almany S, et al. Comparison of coronary angioplasty with compliant and noncompliant balloons (the angioplasty compliance trial). *Am J Cardiol.* 1995;76(7):518-520.
- Salem HK, Gussenhoven EJ, Zhong Y, et al. Effect of balloon angioplasty on femoral artery evaluated with intravascular ultrasound imaging. *Circulation.* 1992;86(2):483-493.
- Chen SL, Guo NS, Chen GD, et al. The immediate elastic recoil of percutaneous coronary angioplasty and intracoronary stent implantation. *J Pract Radiol.* 2001;10:726-728.
- Conti M, Marconi M, Campanile G, et al. Patient-specific finite element analysis of popliteal stenting. *Meccanica.* 2017;52(3):633-644. doi:10.1007/s11012-016-0452-9
- Diamantopoulos A, Katsanos K. Treating Femoropopliteal disease: established and emerging technologies. *Semin Interven. Radiol.* 2014; 31(4):345-352.
- Jaff MR, White CJ, Hiatt WR, et al. An update on Methods for revascularization and expansion of the TASC lesion classification to include below-the-knee arteries: a supplement to the inter-society consensus for the Management of Peripheral Arterial Disease (TASC II). *Vasc Med.* 2015;20(5):465-478.
- Kansal A, Long CA, Patel MR, Jones WS. Endovascular treatment of femoro-popliteal lesions. *Clin Cardiol.* 2019;42(1):175-183.
- Helou B, Bel-Brunon A, Dupont C, et al. Influence of balloon design, plaque material composition, and balloon sizing on acute post angioplasty outcomes: an implicit finite element analysis. *Int J Numer Methods Biomed Eng.* 2021;37(8):e3499-e3522.
- Castaneda-zuniga WR. Pathophysiology of transluminal angioplasty. In: Meyer J, Erberl R, Rupprecht HJ, eds. *Improvement of Myocardial Perfusion.* Martinus Nijhoff; 1985:138-141.
- Holzappel GA, Mulvihill JJ, Cunnane EM, Walsh MT. Computational approaches for analyzing the mechanics of atherosclerotic plaques: a review. *J Biomech.* 2014;47(4):859-869. doi:10.1007/s10865-016-9757-3
- Kiousis DE, Rubinigg SF, Auer M, Holzappel GA. A methodology to analyze changes in lipid Core and calcification onto fibrous cap vulnerability: the human atherosclerotic carotid bifurcation as an Illustratory example. *J Biomech Eng.* 2009;131(12):121002. doi:10.1115/1.4000078
- Li ZY, Howarth S, Trivedi RA, U-King-Im JM, et al. Stress analysis of carotid plaque rupture based on in vivo high resolution MRI. *J Biomech.* 2006;39(14):2611-2622. doi:10.1016/j.jbiomech.2005.08.022
- Auricchio F, Conti M, De BM, De SG, Verheghe B. Carotid artery stenting simulation: from patient-specific images to finite element analysis. *Med Eng Phys.* 2011;33(3):281-289. doi:10.1016/j.medengphy.2010.10.011
- Kiousis DE, Gasser TC, Holzappel GA. A numerical model to study the interaction of vascular stents with human atherosclerotic lesions. *Ann Biomed Eng.* 2007;35(11):1857-1869. doi:10.1007/s10439-007-9357-z
- Holzappel GA, Stadler M, Gasser TC. Changes in the mechanical environment of stenotic arteries during interaction with stents: computational assessment of parametric stent designs. *J Biomech Eng.* 2005;127:166-180.
- Gardiner J, Bonn J, Sullivan KL. Quantification of elastic recoil after balloon angioplasty in the iliac arteries. *J Vasc Interv Radiol.* 2001; 12(12):1389-1393. doi:10.1016/s1051-0443(07)61694-7
- Hanet C, Wijns W, Michel X, Schroeder E. Influence of balloon size and stenosis morphology on immediate and delayed elastic recoil after percutaneous transluminal coronary angioplasty. *J Am Coll Cardiol.* 1991;18(2):506-511. doi:10.1016/0735-1097(91)90607-B

21. Rensing BJ, Hermans WR, Strauss BH, Serruys PW. Regional differences in elastic recoil after percutaneous transluminal coronary angioplasty: a quantitative angiographic study. *J Am Coll Cardiol*. 1991;17(6 suppl. 2):34-38. doi:10.1016/0735-1097(91)90936-4
22. Conway C, McGarry JP, Edelman ER, Al E. Numerical simulation of stent angioplasty with Predilation: an investigation into lesion constitutive representation and calcification influence. *Ann Biomed Eng*. 2017;45:2244-2252. doi:10.1007/s10741-014-9462-7.Natural
23. Holzapfel GA, Stadler M, Schulze-Bauer CA. A layer-specific three-dimensional model for the simulation of balloon angioplasty using magnetic resonance imaging and mechanical testing. *Ann Biomed Eng*. 2002;30(6):753-767. doi:10.1114/1.1492812
24. Gasser TC, Holzapfel GA. Finite element modeling of balloon angioplasty by considering overstretch of remnant non-diseased tissues in lesions. *Comput Mech*. 2007;40:47-60.
25. Decorato I, Kharboutly Z, Legallais C, Salsac AV. Comparison of two endovascular treatments of a stenosed arteriovenous fistula: balloon-angioplasty with and without stenting. *Int J Artif Organs*. 2014;37(10):763-772. doi:10.5301/ijao.5000324
26. Liang DK, Yang DZ, Qi M, Wang WQ. Finite element analysis of the implantation of a balloon-expandable stent in a stenosed artery. *Int J Cardiol*. 2005;104(3):314-318. doi:10.1016/j.ijcard.2004.12.033
27. Yushkevich PA, Piven J, Hazlett C, et al. User-guided 3D active contour segmentation of anatomical structures: significantly improved efficiency and reliability. *Neuroimage*. 2006;31:1116-1128. doi:10.1016/j.neuroimage.2006.01.015
28. Maher E, Creane A, Sultan S, Hynes N, Lally C, Kelly DJ. Inelasticity of human carotid atherosclerotic plaque. *Ann Biomed Eng*. 2011;39(9):2445-2455. doi:10.1007/s10439-011-0331-4
29. Maher E, Early M, Creane A, Lally DJ, Kelly C. Site specific inelasticity of arterial tissue. *J Biomech*. 2012;45(8):1393-1399.
30. Grogan JA, Leen SB, McHugh PE. Comparing coronary stent material performance on a common geometric platform through simulated bench testing. *J Mech Behav Biomed Mater*. 2012;12:129-138.
31. Li D, Robertson AM, Lin G, Lovell M. Finite element modeling of cerebral angioplasty using a structural multi-mechanism anisotropic damage model. *Int J Numer Methods Eng*. 2012;92:457-474. doi:10.1002/nme
32. Kimball BP, Bui S, Cohen EA, Carere RG, Adelman AG. Comparison of acute elastic recoil after directional coronary atherectomy versus standard balloon angioplasty. *Am Heart J*. 1992;124(6):1459-1466. doi:10.1016/0002-8703(92)90057-3
33. Isner J, Rosenfield K, Losordo D, et al. Combination balloon-ultrasound imaging catheter for percutaneous transluminal angioplasty. Validation of imaging, analysis of recoil, and identification of plaque fracture. *Circulation*. 1991;84:739-754.
34. Haude M, Erbel R, Issa H, Meyer J. Quantitative analysis of elastic recoil after balloon angioplasty and after intracoronary implantation of balloon expandable Palmaz-Schatz stents. *J Am Coll Cardiol*. 1993;21:26-34.
35. Ohayon J, Dubreuil O, Tracqui P, et al. Influence of residual stress/strain on the biomechanical stability of vulnerable coronary plaques: potential impact for evaluating the risk of plaque rupture. *Am J Physiol Heart Circ Physiol*. 2007;293:H1987-H1996.
36. Holzapfel GA, Sommer G, Regitnig P. Anisotropic mechanical properties of tissue components in human atherosclerotic plaques. *J Biomech Eng*. 2004;126:657-665.

**How to cite this article:** Helou B, Bel-Brunon A, Dupont C, et al. Patient-specific finite element simulation of peripheral artery percutaneous transluminal angioplasty to evaluate the procedure outcome without stent implantation. *Int J Numer Meth Biomed Engng*. 2023;39(3):e3685. doi:10.1002/cnm.3685

## APPENDIX A

### A.1 | MESH-SIZE SENSITIVITY ANALYSIS

The stenosed artery was meshed by the same element type as in Helou et al.<sup>11</sup> with mixed u-P formulations as well, for the same reason of avoiding volumetric locking and thus enhancing accuracy within the simulations. In the following mesh size sensitivity analysis, the balloon was simulated to a sizing of 5 mm within the patient-specific lipidic stenosis case.

Figure A1 presents the variation of the total strain energy at max balloon inflation and the simulation result file size with respect to different element sizes within the stenosed artery. Toward reducing the simulation computational costs while keeping a satisfying accuracy, element sizes of 0.28 and 0.24 mm, respectively, were chosen to mesh the entire geometry and the stenosed inner surface in contact with the balloon during inflation. Enough elements in the arterial wall thickness were ensured with the selected mesh sizes. Figure A2 shows the distribution of plastic strain along the stenosed artery with the different mesh sizes; their color-maps highlight the insignificant impact of mesh density on the outcomes and also justify our elements sizes choice for the simulations of this patient.

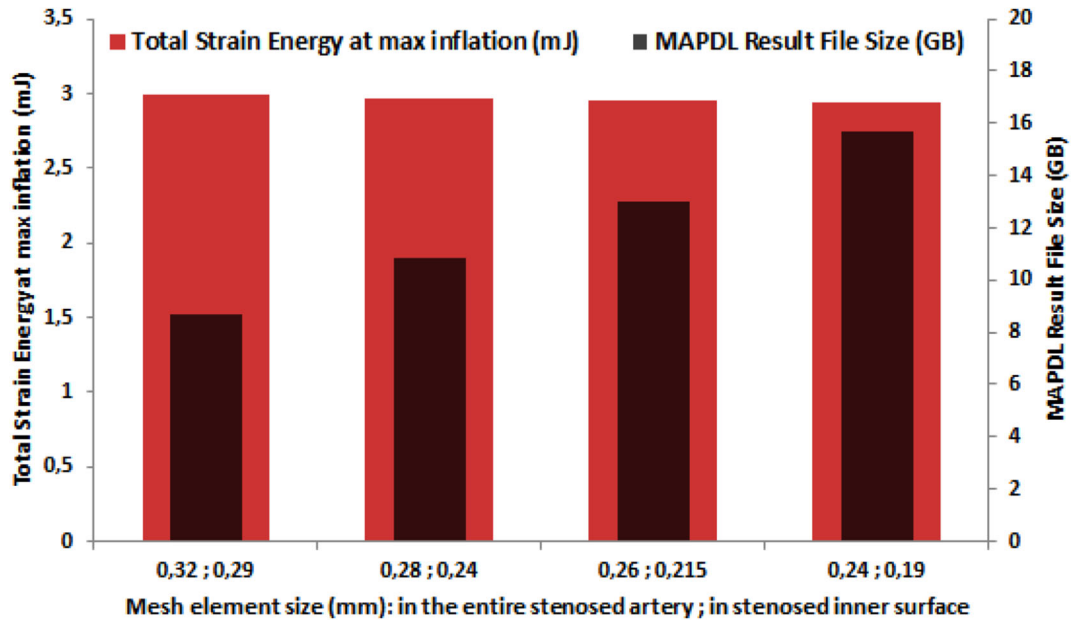


FIGURE A1 Mesh-sizes influence on the total strain energy stored in the diseased arteries at max inflation (diameter of 5 mm), and on their resulting files sizes

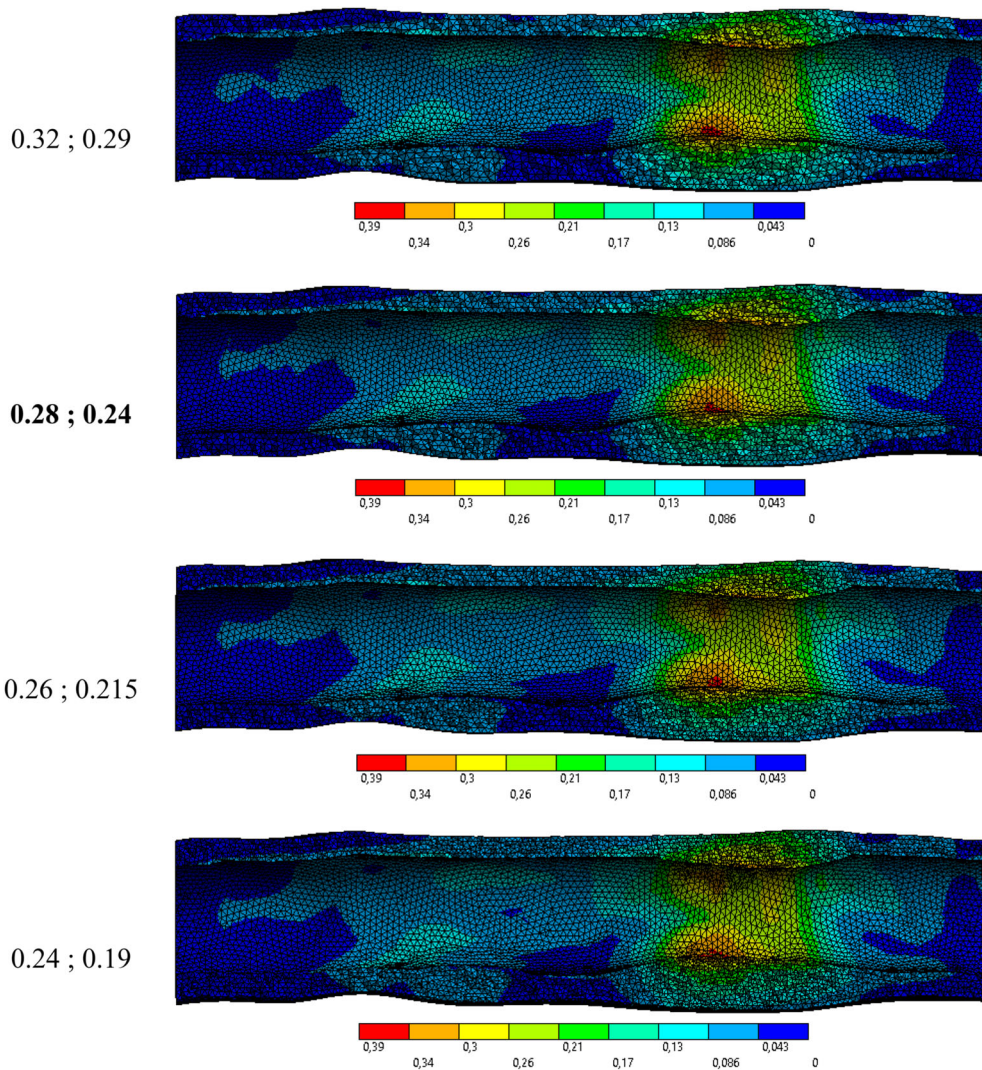


FIGURE A2 Plastic strain distribution along a longitudinal cross-section of the patient-specific geometry corresponding to different element sizes used for meshing the stenosed artery in each simulated case